



Characterization of mechanical properties and microstructures of spark plasma sintered and cryo-rolled AA2024–Y composites

CH. S. VIDYASAGAR¹, D. B. KARUNAKAR²

1. Metallurgical and Materials Engineering Department, Indian Institute of Technology, Roorkee-247667, India;

2. Mechanical and Industrial Engineering Department, Indian Institute of Technology, Roorkee-247667, India

Received 13 December 2019; accepted 9 May 2020

Abstract: The relationship between the microstructure and mechanical properties of the spark plasma sintered AA2024–Y composites subjected to cryo-rolling was investigated. Yttrium addition enhances the mechanical properties of the composites by promoting grain refinement and precipitation. However, there is a clear trend of initial increase and later decrease in the properties. Also, it is observed that 0.3 wt.% of yttrium is the optimum amount of reinforcement content to obtain the highest mechanical properties. To further improve the tensile strength of the composites, cryo-rolling was performed on the composites under standard cryogenic conditions by several passes up to a reduction of 25%. The mechanical properties and the corresponding microstructures of composites after cryo-rolling were correlated. The SEM and TEM microstructures reveal that the samples exhibit dual size grains, i.e., nanograins are formed as sub-grains within the actual grain. Due to the grain size reduction and the increase in the dislocation density, the tensile properties are remarkably improved compared to those of the composites before cryo-rolling. The highest mechanical properties like hardness, YS and UTS are found to be 153 HV, 539 MPa and 572 MPa, respectively, with a reasonable ductility in the composite with 0.3 wt.% Y.

Key words: secondary processing; cryo-rolling; nanograins; yttrium addition; dual size grains; spark plasma sintering

1 Introduction

Currently, there is a rapid rise in demand for light metals and alloys. Light metals like aluminium have the potential to play a vital role in the development of the automotive industry due to their lower density and high specific strength compared to steel [1]. Aluminium has been increasingly used in several applications such as engine blocks, chassis, and rims [2]. However, on earlier, the application of aluminium has one objective, i.e., to reduce weight or replacing thicker sections of the same weight compared to the weight of steel which occupies much space [3,4]. This created new challenges for manufacturers to reach the current demand of providing high-strength, low density and cheap aluminium metals and alloys [4]. However,

there are still some drawbacks regarding the use of aluminium metals and alloys. To overcome these drawbacks, many attempts have been made to boost the properties of aluminium. Examples include alloying [5], the addition of grain modifiers [6,7], the addition of hard ceramics [8–11] to make aluminium composite, heat treatment [12–15], etc. In addition, secondary processes like severe plastic deformation (SPD) such as accumulative roll bonding [16,17], cryo-rolling [18–21], cryo-forging [22,23], hot forging [24], forging [25], equi-channel angular processing [26,27], and high torsion [28,29] have also become necessary to reduce grain size. SPD processes have been developed as early as the 1990s to produce bulk ultra-fine grained (UFG) metals and alloys.

Recently, rapidly solidified RS–Al–TM (TM= Transition metal) composites have been reported to

exhibit a tensile strength of 1200 MPa, which is more than double the strength of a commercial aluminium alloy [30].

The behavior of aluminium and its alloys has been extensively studied concerning their mechanical properties under cryo-rolling conditions. However, very little or no literature is available on the behavior of cryo-rolled aluminium composites. Therefore, the present study focuses on the effect of cryo-rolling on the spark plasma sintered AA2024–Y micro composites. A pure spark plasma sintered AA2024 was also cryo-rolled as a benchmark for comparison.

The micro composite samples developed through SPS with AA2024 as the matrix material and varying contents of yttrium as the reinforcement were further subjected to SPD to improve their strength. The method of SPD employed in the present study was rolling at cryogenic temperature (cryo-rolling).

2 Experimental

2.1 Starting materials

In the present work, the powders of AA2024 and micro yttrium were selected as the matrix and

reinforcing material, respectively. The approximate elemental composition of the as-received AA2024 starting powder is given in Table 1.

Table 1 Chemical composition of as-received AA2024 powder (wt.%)

Si	Cu	Fe	Zn	Mg	Ti	V	Mn	Al
0.16	4.67	0.47	0.14	1.71	0.05	0.001	0.8	Bal.

This AA2024 powder with an average particle size of 60 μm was purchased from Alfa Aesar (United States), which was processed through gas atomization. Figure 1 shows the starting as-received powders of AA2024, yttrium, schematic diagram of the intended spark plasma sintered composite sample and composite samples after SPS.

The as-received powders of AA2024 and yttrium were examined by SEM and their microstructures are shown in Figs. 1(a) and (b), respectively. The microstructure reveals a near-spherical morphology of Al particles, as seen from Fig. 1(a). Yttrium powder with the largest particle size of 420 μm is used as reinforcement. This yttrium powder (99.6% in purity with a maximum of 0.4% rare earth oxide impurities) is procured

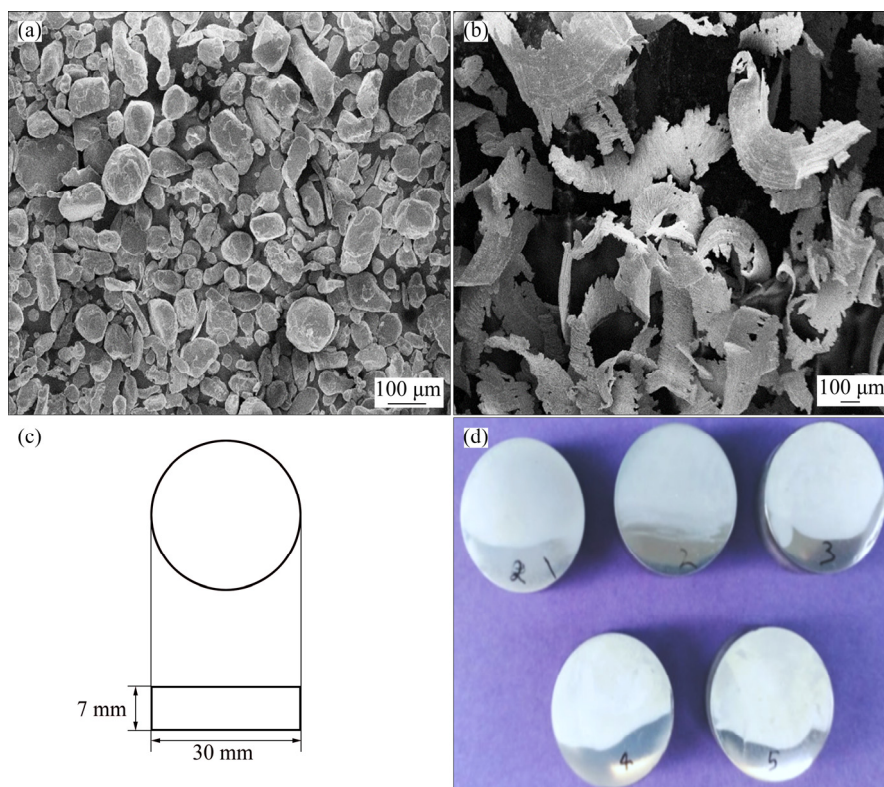


Fig. 1 Starting as-received powders of AA2024 (a), yttrium (b), schematic diagram of intended spark plasma sintered composite sample (c) and composite samples after SPS (d)

from Alfa Aesar (United States). The microstructure of loose yttrium powder is shown in Fig. 1(b). From Fig. 1(b), it can be observed that the morphology of yttrium particles is like ribbons or chips having three different dimensions.

2.2 Preparation of composite and cryo-rolling

Five AA2024 matrix composite samples reinforced with different proportions of yttrium have been prepared along with a pure AA2024 specimen. These SPS specimens were developed in our previous work [31] and the details of results and discussion are not given here. The intended compositions of the composite samples are given in Table 2.

Table 2 Intended compositions of different composite samples

Sample No.	Content/wt.%	
	AA2024	Yttrium
1	100	–
2	99.9	0.1
3	99.8	0.2
4	99.7	0.3
5	99.6	0.4
6	99.5	0.5

For the uniform mixing of the matrix and the reinforcement powders, a planetary ball-milling machine is used. The planetary ball mill is operated at 50 r/min for 2 h with a ball to powder ratio of 1:1. From Fig. 2, it can be observed that the powder particles were not deformed plastically, but were mixed properly during milling of powders in the ball mill. The blended composite powders were consolidated into samples with diameter of 30 mm and thickness of 7 mm by SPS with the parameters given in Table 3. SPS process was carried out using Dr. Sinter SPS-625, Fuji Electronic Industrial Co., Ltd. (Japan).

The composite samples developed through SPS were further subjected to cryo-rolling. The samples were cryo-rolled to a 25% reduction at $-196\text{ }^{\circ}\text{C}$. The samples were carefully rolled with a 1% reduction in each pass. After each pass, the composite samples were immersed in liquid nitrogen to attain and maintain the cryogenic temperature.

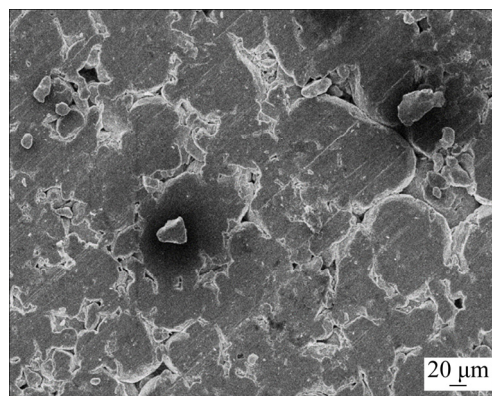


Fig. 2 FE-SEM microstructure of SPS sintered sample with 0.3 wt.% yttrium addition

Table 3 SPS parameters employed to sinter composite powders

Parameter	Value
Heating rate/ $(^{\circ}\text{C}\cdot\text{min}^{-1})$	50
Sintering temperature/ $^{\circ}\text{C}$	450
Holding time/s	180
Cooling rate/ $(^{\circ}\text{C}\cdot\text{min}^{-1})$	100
Pressure/MPa	50

In the present study, the metallurgical characterization was performed by OM, FE-SEM and TEM. After SPS and cryo-rolling, the SPS samples were cut into convenient pieces and were polished using 800, 1200, 1600 and 2000 grade SiC emery papers. Then, the samples were cloth polished using a diamond paste until mirror polish was obtained. The mirror-polished samples were etched for 30–40 s with a modified Keller's reagent which was prepared by mixing 10 mL HNO_3 , 1.5 mL HCl , 1 mL HF and 87.5 mL distilled water. The etched samples were observed under various microscopes to obtain appropriate microstructures.

The optical microscopy was carried out using a LEICA DMI 5000M (Leica Microsystems, Buffalo Grove, IL) microscope. To observe the microstructures at higher magnification, a field emission scanning electron microscope (FE-SEM) (Model: Carl Zeiss ultra plus) equipped with EDS was used. Further, the samples were examined through a high-resolution transition electron microscope (HR-TEM) to investigate the nanograins and dislocation densities. Samples for TEM analysis were prepared by slicing a thin section from the cross-section of the composite

samples by slow diamond cutting which was further thinned down gradually to 100 μm by slow hand polishing. Then, circular discs of 3 mm in diameter were cut from the thinned slice and the discs were further thinned by using a dimple grinder with diamond paste. Finally, the dimpled discs were electropolished using a twin-jet electro polishing set-up with 75% CH_3OH and 25% HNO_3 solution at 12 V and -35°C .

3 Results

3.1 Microstructure observation

Based on our previous work, the sample with 0.3 wt.% yttrium addition showed better mechanical properties. Figure 2 shows the microstructure of the sample with 0.3 wt.% yttrium addition.

The mechanical properties of the SPS sintered composites before cryo-rolling developed in our previous study are given in Table 4.

Figure 3 shows the FE-SEM microstructures of the cross-sections of the cryo-rolled composite sample with varying amounts of yttrium.

It can be observed from Fig. 3 that cryo-rolling induced severe stress and strain through the action of compression in the composite samples. The grains got compressed and took the shape of a honeycomb with an approximate hexagonal structure. Almost all the grains were of similar shape and size in each composite sample. Cryo-rolling also introduced high dislocation density, which can be seen along the grain boundaries. From Fig. 3(c), it can be observed that the matrix grains tended to become smaller with 0.2 wt.% yttrium reinforcement as encircled in white on the microstructure. As yttrium reinforcement content reached 0.3 wt.%, the number of smaller grains

increased and spread throughout the matrix, as observed in Fig. 3(d) encircled in white. With further increase in yttrium content, the smaller grains disappeared. The grain sizes of the cryo-rolled composite samples were calculated by the linear intercept method and confirmed by IMAGE J software. The calculated grain sizes were 8, 4, 3, 1, 4 and 5 μm for the samples 1–6, respectively. Figure 4 shows the optical microstructures of the longitudinal sections of the samples.

Although all the microstructures look alike, from Fig. 4, it can be observed that the grains were elongated in the rolling direction (shown by a black arrow) in Fig. 4(a) and the induced strain was also able to cut the elongated grains as the yttrium content was increased up to 0.3 wt.%. Rolling induced a high number of dislocations in the composite samples and the generated dislocations piled up at the grain boundaries as observed in the microstructures. The elongated grain size tended to decrease in the composite samples up to 0.3 wt.% yttrium addition. Upon further increase in yttrium reinforcement, the grain size increased.

For further analysis, the FE-SEM microstructure of the composite sample reinforced with 0.3 wt.% yttrium was considered. The microstructure was taken in the direction perpendicular to the rolling direction, as shown in Fig. 5. Due to the severe plastic deformation achieved in the composite sample by cryo-rolling, the grains and the subgrains were compressed. As a result of the compression action in the composite sample, subgrains were formed within the normal grains, and nanograins were formed within the subgrains as highlighted with a red circle in Fig. 5. Since the cryo-rolling process suppressed the dynamic re-crystallization, the shape and size of the grains were retained after rolling.

Table 4 Mechanical properties of SPS sintered samples before cryo-rolling

Sample No.	Composition	Hardness (HV)	YS/MPa	UTS/MPa	Elongation/%
1	AA2024	101 \pm 7	143 \pm 11	226 \pm 16	14.3 \pm 1.3
2	AA2024–0.1wt.%Y	108 \pm 3	221 \pm 25	287 \pm 31	14.9 \pm 2.2
3	AA2024–0.2wt.%Y	112 \pm 4	262 \pm 23	315 \pm 42	17.1 \pm 2.7
4	AA2024–0.3wt.%Y	114 \pm 3	343 \pm 26	388 \pm 32	18.4 \pm 3.1
5	AA2024–0.4wt.%Y	110 \pm 3	337 \pm 12	359 \pm 18	16.5 \pm 2.6
6	AA2024–0.5wt.%Y	109 \pm 5	311 \pm 25	342 \pm 35	16.2 \pm 0.9

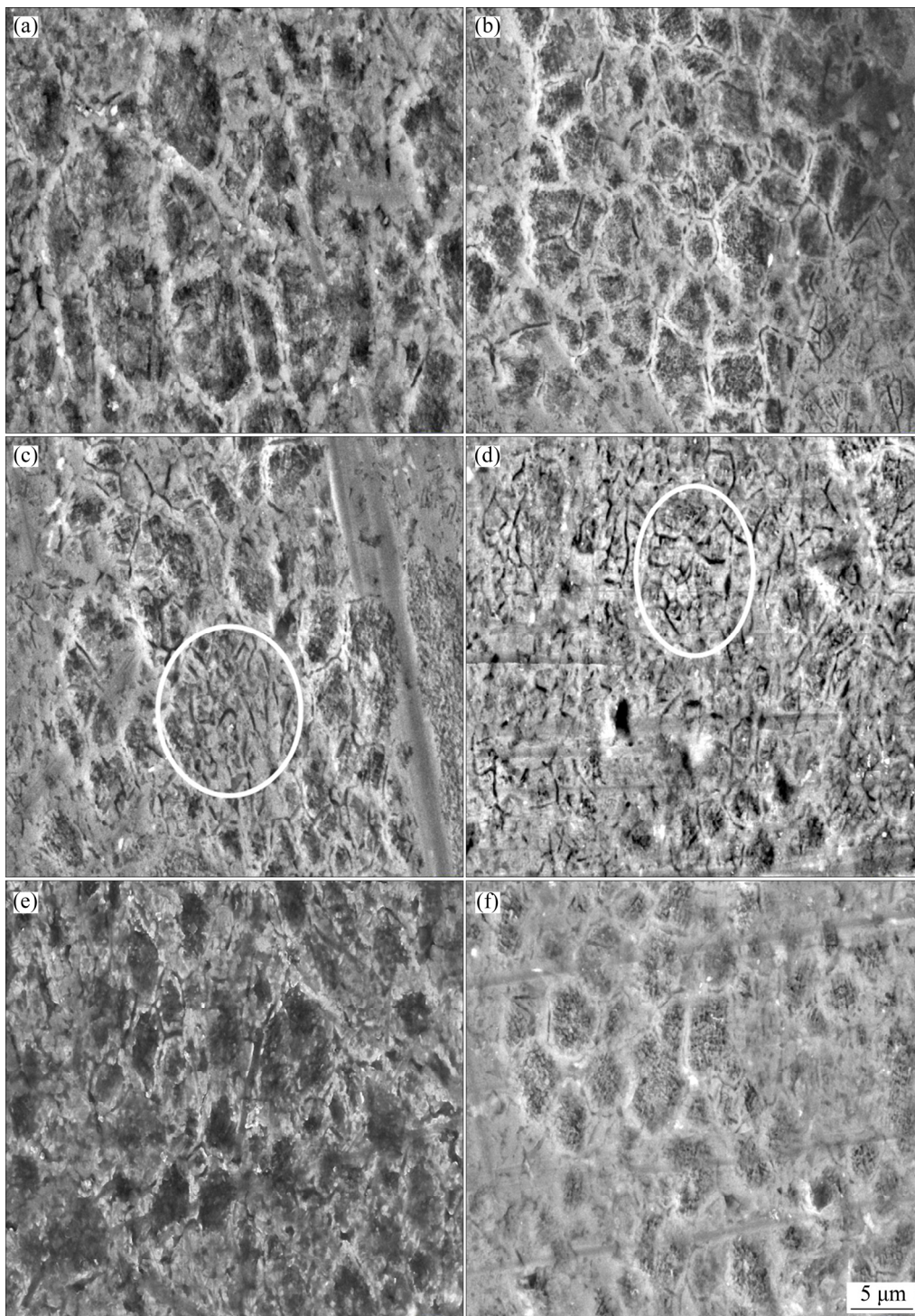


Fig. 3 FE-SEM microstructures of cross-sections of SPSed and cryo-rolled composite samples in direction perpendicular to rolling: (a) Sample 1; (b) Sample 2; (c) Sample 3; (d) Sample 4; (e) Sample 5; (f) Sample 6 (White circles in (c) and (d) show sub-grains)

Figure 6 shows the TEM nanostructures of the cryo-rolled composite samples with varying amounts of yttrium reinforcement.

From Fig. 6, the formation of nanograins due to cryo-rolling can be observed. The nano grain size decreased from a few tens of nanometers to a few

nanometers with variation in yttrium content from 0.1 to 0.3 wt.%. With further increase in the yttrium content, the grains tended to coarsen. The dislocation density achieved in the composite samples by cryo-rolling can be observed as dark clouds in the nanostructures.

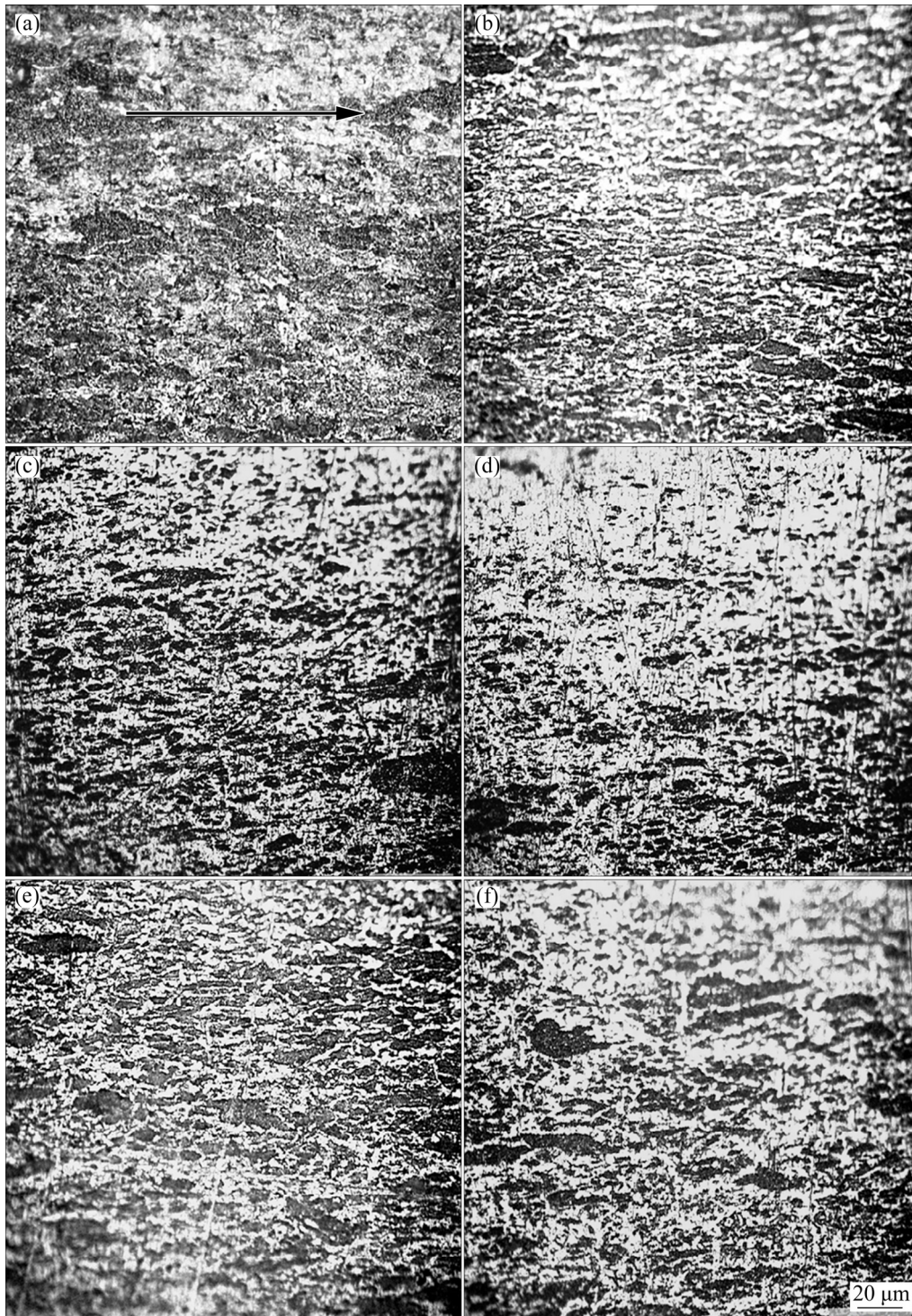


Fig. 4 Optical microstructures of SPSed and cryo-rolled composite samples in longitudinal rolling direction: (a) Sample 1; (b) Sample 2; (c) Sample 3; (d) Sample 4; (e) Sample 5; (f) Sample 6 (Black arrow in (a) shows rolling direction)

For further investigation of the shape and size of the nanograins, the TEM nanostructure of the composite sample with 0.3 wt.% yttrium reinforcement was taken at a higher magnification. Figure 7 shows the TEM nanostructure of the composite sample with 0.3 wt.% yttrium

reinforcement at higher magnification.

The black arrow on the nanostructure indicates the cryo-rolling direction. From the nanostructure in Fig. 7, it can be observed that the nanograins had an ellipsoid shape and were about 10 nm in size. Almost all the grains had similar shape and size.

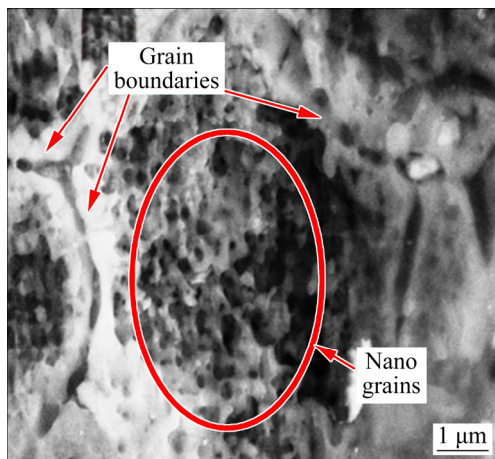


Fig. 5 FE-SEM microstructure of SPSed and cryo-rolled composite sample reinforced with 0.3 wt.% yttrium showing formation of nanograins (Red circle and arrows denote nanograins and grain boundaries, respectively)

3.2 Evaluation of mechanical properties

The mechanical properties of the cryo-rolled composite samples such as hardness, UTS, YS and elongation were determined as per the standard procedure. The hardness was taken on the rolled surfaces and the tensile testing was done on the samples in the rolling direction.

Figure 8 shows the hardness variation of the cryo-rolled composite samples with varying

amounts of yttrium. Rolling induced a large number of dislocations in the composite, whose movement became difficult with the reduction in grain size, dispersion of reinforcement and precipitates, hence increasing the hardness of the composite samples. The cryogenic temperature played an important role in suppressing the recrystallization and grain growth, retaining the grain size during and after rolling by absorbing the heat energy responsible for grain growth.

The hardness of the cryo-rolled composite samples followed the same trend as the hardness of the composite samples developed through other processing techniques, as discussed earlier. The hardness achieved can be attributed to the increase in dislocation density due to rolling. The highest hardness of 153 HV is achieved for the spark plasma sintered and cryo-rolled composite sample with 0.3 wt.% yttrium addition. With further increase in yttrium content, the hardness tended to decrease. Compared to the hardness of the composite samples developed through stir casting, cold compaction and spark plasma sintering, cryo-rolled composite samples exhibited a significant increase in hardness.

Three tensile samples were cut from each sample of the spark plasma sintered and cryo-rolled

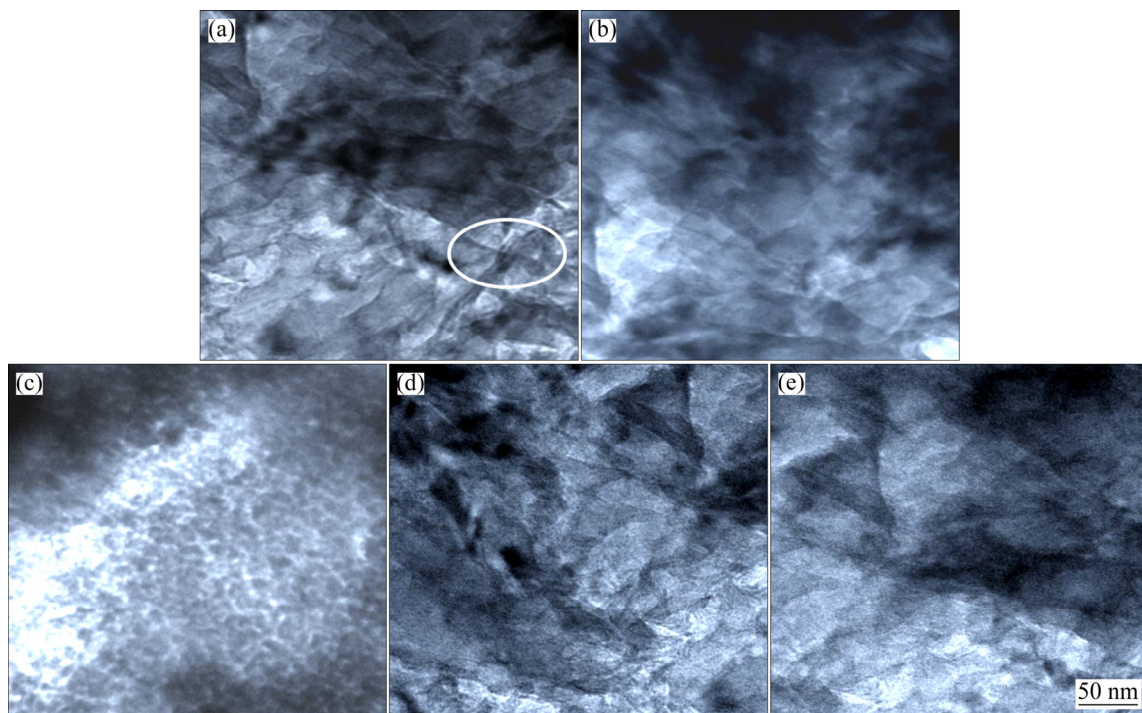


Fig. 6 TEM nanostructures of cross-sections of SPSed and cryo-rolled composite samples in direction perpendicular to rolling: (a) Sample 1; (b) Sample 2; (c) Sample 3; (d) Sample 4; (e) Sample 5; (f) Sample 6 (White circle in (a) denotes a triple grain boundary junction)

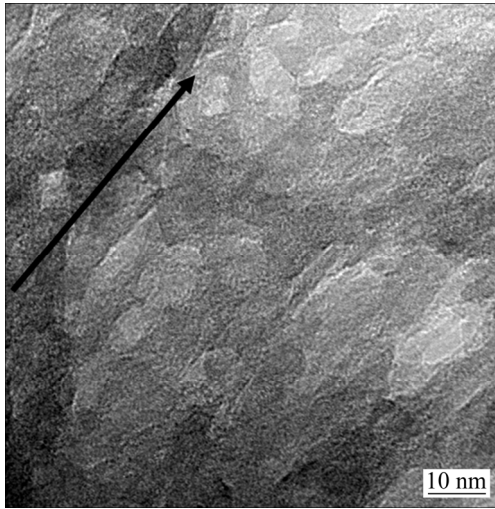


Fig. 7 TEM nanostructure of SPSed and cryo-rolled composite sample reinforced with 0.3 wt.% yttrium at higher magnification (Black arrow shows direction of rolling)

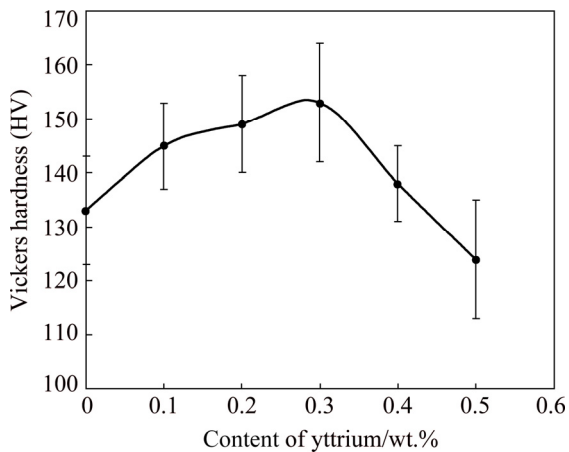


Fig. 8 Hardness variation of SPSed and cryo-rolled composite samples reinforced with varying contents of yttrium

composite and the tensile test was done according to the standard procedure. The UTS and YS of the cryo-rolled composite samples are shown in Fig. 9. It can be noted that both the hardness and tensile properties of the cryo-rolled composite samples followed the same trend of variation as the un-rolled composite samples. The UTS and YS of the spark plasma sintered composite samples increased remarkably by cryo-rolling. Compared to unrolled spark plasma sintered composite samples, there was an increase in both UTS and YS of the cryo-rolled composite samples. However, unlike the un-rolled composite samples, the decrease in tensile strength was steep.

The highest UTS and YS reached up to 572 and 539 MPa, respectively, for the cryo-rolled composite sample with 0.3 wt.% yttrium reinforcement. With further increase in yttrium content, the UTS and YS decreased. The variation in the elongation of the cryo-rolled composite samples with yttrium addition is shown in Fig. 10.

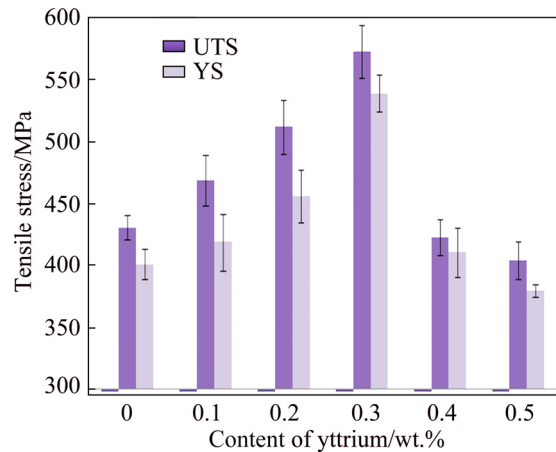


Fig. 9 Variation of UTS and YS for SPSed and cryo-rolled composite samples reinforced with varying contents of yttrium

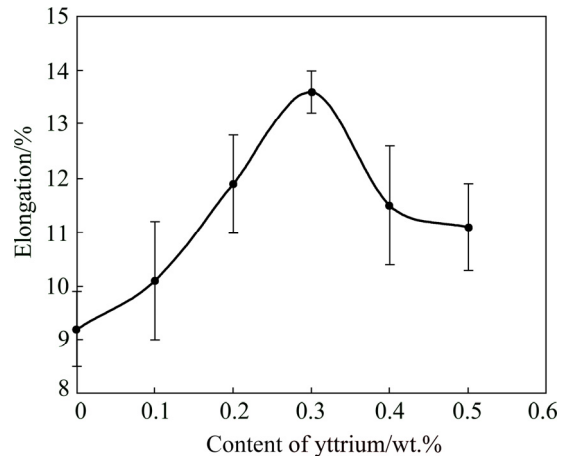


Fig. 10 Variation of elongation of SPSed and cryo-rolled composite samples reinforced with varying contents of yttrium

From Fig. 10, it can be observed that the elongation increased up to 0.3 wt.% yttrium reinforcement and tended to decrease thereafter. The highest elongation achieved in the cryo-rolled composite sample with 0.3 wt.% yttrium reinforcement was 13.6%. Compared to the un-rolled spark plasma sintered composite samples and the composite samples developed through stir casting and cold compaction, the elongation of the cryo-rolled composite samples at fracture was

considerably less. Hence, cryo-rolling should be followed by heat treatment to increase the ductility of the composite samples to a reasonable level.

4 Discussion

Relative density >99.75% was achieved in the composites developed through SPS. The SPS parameters employed in this study could yield densities up to 99.8%, as reported by YAMAOGU et al [32]. The use of cryogenic treatment to improve the mechanical properties of metals and alloys has been developed during the period 1960–1970 [19]. Recently, the application of cryo treatment, especially cryo-rolling, has spread in developing various metal alloys. In the present study, cryo-rolling is applied to aluminium composites sintered through SPS.

The main drawback encountered in the products processed through powder metallurgy is the porosity [33]. In conventional sintering methods, a decrease in the green density due to improper application of pressure and decrease in the sintered density due to poor sintering conditions lead to an increase in the porosity and a decrease in the density [34]. Consolidation of the AA2024–yttrium powders through spark plasma sintering has dramatically increased the density of composite samples due to the simultaneous application of rapid heat and high pressure. When rapid heating and high pressure are applied simultaneously, localized melting and evaporation occurs at the particle interfaces leading to high densification. Moreover, the higher heating rates do not provide enough time and room for recrystallization and grain growth during sintering. Further, in the present study, cryo-rolling of these spark plasma sintered composites led to the suppression of the voids, and hence, it is believed that the samples achieved full densification.

The mechanical properties such as hardness, UTS, YS and elongation of the spark plasma sintered samples (AA2024–Y) before cryo-rolling followed a trend of initial increase and later decrease as seen from Table 4. These properties increased with an increase in the yttrium addition up to 0.3 wt.% and decreased later on. The variation in the properties of the spark plasma sintered samples can be attributed to the grain refinement, fine precipitation and increase in the dislocation

density. Beyond 0.3 wt.% yttrium addition, the effect of grain refinement fades away leading to the grain growth, the Al_2Cu precipitation in the $\alpha(Al)$ matrix coarsens, and therefore, the mechanical properties reduce [31]. Hence, it can be concluded that 0.3 wt.% yttrium is the optimum amount that is capable of creating favorable conditions for grain refinement, precipitation and dislocation growth during sintering.

From Figs. 3 and 4, the grains and grain boundaries of the composite samples after cryo-rolling can be observed. Compared to the starting powders that had an average size of 60 μm and irregular shape and the SPS sintered samples that exhibited spherical grains, the cryo-rolled grains exhibited a typical hexagonal shape due to rolling. The hexagonal structures of the grains denote the uniform pressure/compression applied during rolling. The formation of smaller and equal-sized grains increased the strength of the composite according to the Hall–Petch relation. Rolling includes compressive stress on the material, which crushes the larger grains into several smaller grains. The grains also tended to elongate in the direction of rolling and broke into several smaller grains, as shown in Fig. 4. During rolling, a high amount of heat develops in the material which helps the grains to retain their original size and shape to an extent by the dynamic recrystallization followed by grain growth. In cryo-rolling, the material was at cryogenic temperature, and hence, all the heat developed during rolling was dissipated according to the third law of the thermodynamics, suppressing the dynamic recrystallization.

It is well known that rolling is a type of severe plastic deformation (SPD). Whenever a sample undergoes rolling, it is subjected to a high level of deformation. Due to this deformation, a large number of dislocations [35] are induced in the composite after rolling. The movement of these dislocations became difficult as the overall grain boundary length and the dispersion of reinforcement and precipitates increase. Hence, the mechanical properties of the composite samples increase. When the sample reaches cryogenic temperature, it becomes very brittle, and is difficult to roll without breaking. Therefore, very low reductions were employed in the present work. As the sample is brittle, due to the rolling-induced load, the grains in the matrix tend to break into

several smaller grains. These small grains further break into several nanograins. However, during cryo-rolling, the broken grains do not recrystallize, diffuse or grow into bigger grains as those in room temperature or hot rolling. The steps of dynamic recrystallization and grain growth are completely bi-passed in cryo-rolling. Cryogenic temperature plays an important role in suppressing the recrystallization and grain growth, retaining the grain size during and after rolling by absorbing the heat energy responsible for grain growth. The sample with 0.3 wt.% yttrium addition exhibited the highest degree of grain size reduction, which favored the formation of nanograins during cryo-rolling due to the increase in the number of grains and grain boundary length per unit area. Moreover, with 0.3 wt.% yttrium addition, finely distributed Al_2Cu precipitates were found in the matrix, which could have acted as nodal points for the formation of new smaller grains during cryo-rolling. Beyond 0.3 wt.% yttrium addition, the precipitation coarsened and the number of precipitates per unit area also decreased.

It has been observed that the reinforcement of yttrium to AA2024 matrix and processing through spark plasma sintering caused grain size reduction in the composite samples. The same composite samples after cryo-rolling also exhibited a great deal of grain size reduction. The hardness of the cryo-rolled composite samples increased with an increase in the yttrium reinforcement up to 0.3 wt.% and tended to decrease with a further increase. There was a clear trend of increase and subsequent decrease in the hardness after the cryo-rolling, besides, the cryo-rolling parameters being the same for all the composites. The variation in the hardness of the samples followed the same trend as that of the samples before cryo-rolling, i.e., the samples exhibited the same hardness trend before and after cryo-rolling. However, cryo-rolling enhanced the hardness of the samples as compared to that of the samples before cryo-rolling. Hence, the change in the hardness was clearly because of the yttrium reinforcement. The effect of yttrium reinforcement on the mechanical properties was discussed in our earlier paper [31]. However, the hardness variation can be explained by the Hall–Petch relation. The grain size of the cryo-rolled samples reduced with the addition of yttrium content up to 0.3 wt.%, and hence, the

hardness increased. Beyond 0.3 wt.% yttrium content, the grain size tended to increase and so, the hardness also decreased.

The tensile properties of the cryo-rolled composite samples followed the same trend as the hardness of the composite samples after cryo-rolling. The tensile properties achieved can be attributed to the increase in the dislocation density and grain size reduction achieved by cryo-rolling. The highest tensile properties were achieved in the spark plasma sintered and cryo-rolled composite sample with 0.3 wt.% yttrium addition. With further increase in yttrium content, beyond 0.3 wt.%, the tensile properties tended to decrease. From Fig. 9, it can be observed that the UTS and YS also have increased remarkably by cryo-rolling. The tensile strength achieved in the cryo-rolled composite samples was almost twice that of the un-rolled composite samples as seen from Fig. 9 and Table 4. Due to cryo-rolling, a homogeneous microstructure was achieved with equal size grains throughout. The main mechanisms involved in the strengthening of the cryo-rolled composites were grain boundary strengthening and dislocation strengthening. Both the mechanisms were greatly initiated and activated by cryo-rolling. Cryo-rolling decreased the grain size and induced a high density of dislocations in the composites. Compared to the composite samples developed through stir casting [36] and spark plasma sintering, the SPS sintered samples that were cryo-rolled exhibited a significant increase in the mechanical properties.

Although the tensile properties of the cryo-rolled samples increased, the ductility of the samples decreased drastically. Hence, cryo-rolling should be followed by a heat treatment to increase the ductility of the composite samples to a reasonable level. However, the reason for the retained ductility in the present work could be anyone or a combination of the following reasons:

- (1) Bigger grains and nanograins are present together as the smaller grains contribute to strength, and the bigger grains contribute to ductility [37].

- (2) It is well known that the slip plane of aluminium in $\{111\}$ and the formation of more density of dislocations (seen as a black cloud in Fig. 4) around the slip plans could hinder the slip and crack propagation [36,38].

- (3) The high density of the composites (full density) does not give an easy opportunity for the

slip or crack propagation, which leads to failure as there are no voids. Although the above arguments are properly sited, they also seem to be our hypothesis. The study is not complete and it gives ample scope for researchers for further investigations. Also, further annealing could improve the ductility but only at the cost of strength.

5 Conclusions

(1) Cryo-rolling induced a high amount of dislocation density and significantly decreased the grain sizes throughout the microstructures of the composite samples.

(2) Dual grains of different sizes were observed in the cryo-rolled composite samples. A combination of ultrafine grains and nanograins was present together in the microstructures. The grain sizes of both the ultrafine grains and nanograins got reduced with the reinforcement of yttrium up to 0.3 wt.% and increased with further increase.

(3) The tensile properties of the composite samples increased due to cryo-rolling. The hardness, UTS and YS of the composite samples varied with the variation in respective grain sizes. The highest hardness, UTS and YS achieved were 153 HV, 572 MPa, and 539 MPa, respectively, with an elongation of 13.6% for the cryo-rolled composite sample reinforced with 0.3 wt.% yttrium.

(4) The highest hardness, UTS and YS achieved for the cryo-rolled composites were 115%, 132% and 134% higher compared to those of the unreinforced cryo-rolled sample and 134%, 147% and 157% higher compared to those of the unrolled composite reinforced with 0.3 wt.% yttrium.

Acknowledgments

The authors would like to thank the Indian Institute of Technology Roorkee and MHRD for providing financial support and laboratory facilities.

References

- [1] MEKONNEN A F, MAHMUT A S. Materials used in automotive manufacture and material selection using Ashby charts [J]. *International Journal of Materials Engineering*, 2018, 8(3): 40–54. doi: 10.5923/j.ijme.20180803.02.
- [2] HIRSCH J. Aluminium in innovative light-weight car design [J]. *Mater Trans*, 2011, 52: 818–824. doi.org/10.2320/matertrans.L-MZ201132.
- [3] OLOYEDE O. Feasibility of replacing structural steel with aluminum alloys in the commercial shipbuilding industries in Nigeria [J]. *International Journal of Science and Technological Research*, 2012, 9: 188–204.
- [4] TISZA M, CZINEGE I. Comparative study of the application of steels and aluminium in lightweight production of automotive parts [J]. *Int J Light Mater Manuf*, 2018, 1: 229–238. <https://doi.org/10.1016/j.ijlmm.2018.09.001>.
- [5] DAVIS J R. Alloying: Understanding the basics [M]. ASM International, 2001: 351–416. <https://doi.org/10.1361/autb2001p351>.
- [6] RATHOD N R, MANGHANI J V. Effect of modifier and grain refiner on cast Al-7Si aluminum alloy: A review [J]. *Int J Emerg Trends Eng Dev*, 2012, 5: 574–582.
- [7] MALLAPUR D G. Influence of grain refiner and modifier on the microstructure and mechanical properties of A356 Alloy [J]. *Int J Eng Sci Technol*, 2010, 2: 4487–4493.
- [8] AJAGOL P, ANJAN B N, MARIGOUDAR R N, PREETHAM G V. Effect of SiC reinforcement on microstructure and mechanical properties of aluminum metal matrix composite [C]//IOP Conference Series: Materials Science and Engineering. Badaga Mijar, Moodbidri, Karnataka, India, 2018, 376: 012057. <https://doi.org/10.1088/1757-899X/376/1/012057>.
- [9] MOHAMMED M M, ELKADY O A, ABDELHAMEED A W. Effect of alumina particles addition on physico-mechanical properties of Al-matrix composites [J]. *Open J Met*, 2013, 3: 72–79. <https://doi.org/10.4236/ojmetal.2013.34011>
- [10] SHARMA P, SHARMA S, KHANDUJA D. Production and some properties of Si₃N₄ reinforced aluminium alloy composites [J]. *J Asian Ceram Soc*, 2015, 3: 352–359. <https://doi.org/10.1016/j.jascer.2015.07.002>.
- [11] PULKIT G, ANBESH J, DEVENDRA K, KISHOR K S, CHAUDHERYM H, PALLAV G. Advance research progresses in aluminium matrix composites: manufacturing & applications [J]. *Journal of Materials Research and Technology*, 2019, 8(5): 4924–4939. <https://doi.org/10.1016/j.jmrt.2019.06.028>.
- [12] ZHANG Peng-xiang, HONG Yan, WEI Liu, ZOU Xiu-liang, TANG Bin-bing. Effect of T6 heat treatment on microstructure and hardness of nanosized Al₂O₃ reinforced 7075 aluminum matrix composites [J]. *Metals*, 2019, 9(44): 1–12. doi:10.3390/met9010044.
- [13] ROSELINE S, PARAMASIVAM V. Corrosion behaviour of heat treated aluminium metal matrix composites reinforced with fused zirconia alumina 40 [J]. *Journal of Alloys and Compounds*, 2019, 799: 205–215. <https://doi.org/10.1016/j.jallcom.2019.05>.
- [14] ZEREN M. The effect of heat-treatment on aluminum-based piston alloys [J]. *Mater Des*, 2007, 28: 2511–2517. <https://doi.org/10.1016/j.matdes.2006.09.010>.
- [15] ISADARE A D, AREMO B, ADEOYE M O, OLAWALE O J, SHITTU M D. Effect of heat treatment on some

- mechanical properties of 7075 aluminium alloy [J]. *Mater Res*, 2013, 16: 190–194. <https://doi.org/10.1590/S1516-14392012005000167>.
- [16] SEYED M G, MASSOUD M, MANOJ G. Accumulative roll bonding—A review [J]. *Appl Sci*, 2019, 9: 1–32. doi:10.3390/app9173627.
- [17] TANG Yong-peng, SHOICHI H, SEIJI S, KENJI M, LEE Seungwon, ZENJI H, DAISUKE T. Microstructures and the mechanical properties of the Al–Li–Cu alloy strengthened by the combined use of accumulative roll bonding and aging [J]. *Advanced Engineering Materials*, 2019, 22: 1–13. <https://doi.org/10.1002/adem.201900561>.
- [18] HUANG Y C, YAN X Y, QIU T. Microstructure and mechanical properties of cryo-rolled AA6061 Al alloy [J]. *Trans Nonferrous Met Soc China*, 2016, 26: 12–18. [https://doi.org/10.1016/S1003-6326\(16\)64083-9](https://doi.org/10.1016/S1003-6326(16)64083-9).
- [19] SATISH D R, FEYISSA F, KUMAR D R. Cryorolling and warm forming of AA6061 aluminum alloy sheets [J]. *Mater Manuf Process*, 2017, 32: 1345–1352. <https://doi.org/10.1080/10426914.2017.1317352>.
- [20] YU H L, LU C, TIEU K, LIU X H, SONG Y, YU Q B, KONG C. Asymmetric cryo-rolling for fabrication of nanostructural aluminum sheets [J]. *Sci Rep*, 2012, 2: 1–5. <https://doi.org/10.1038/srep00772>.
- [21] MARNETTE J, WEISS M, HODGSON P D. Roll-formability of cryo-rolled ultrafine aluminium sheet [J]. *Mater Des*, 2014, 63: 471–478. <https://doi.org/10.1016/j.matdes.2014.06.036>.
- [22] SHIH T S, LIAO T W, HSU W N. Effects of cryogenic forging and anodization on the mechanical properties of AA 7075-T73 aluminum alloys [J]. *J Mater Eng Perform*, 2016, 25: 1211–1218. <https://doi.org/10.1007/s11665-016-1946-2>.
- [23] AZIMI A, OWOLABI G M, FALLAHDOST H, KUMAR N, WHITWORTH H, WARNER G. AA2219 aluminum alloy processed via multi-axial forging in cryogenic and ambient environments [J]. *J Mater Sci Res*, 2019, 8: 1–10. <https://doi.org/10.5539/jmsr.v8n2p1>.
- [24] PUROHIT R, QURESHI M M U, RANA R S. The effect of hot forging and heat treatment on wear properties of Al6061–Al₂O₃ nano composites [J]. *Mater Today Proc*, 2017, 4(2): 4042–4048. <https://doi.org/10.1016/j.matpr.2017.02.306>.
- [25] NAKAI M, ITOH G. The effect of microstructure on mechanical properties of forged 6061 aluminum alloy [J]. *Mater Trans*, 2014, 55: 114–119. <https://doi.org/10.2320/matertrans.MA201324>.
- [26] JAIRO A M, OSCAR F H, VANINA T, PABLO R, MARTINA A, RAUL E B. Equal channel angular sheet extrusion (ECASE) as a precursor of heterogeneity in an AA6063-T6 alloy [J]. *The International Journal of Advanced Manufacturing Technology*, 2019, 102: 3459–3471. <https://doi.org/10.1007/s00170-019-03425-7>.
- [27] SALLEH M S, ISHAK N N M, YAHAYA S H, SUBRAMONIAN S, ABDULLAH A. Effect of equal channel angular pressing on the microstructure and mechanical properties of A356 alloy [J]. *The International Journal of Advanced Manufacturing Technology*, 2018, 12: 79–91.
- [28] KAWASAKI M, AHN B, LEE H. Using high-pressure torsion to process an aluminum-magnesium nanocomposite through diffusion bonding [J]. *J Mater Res*, 2016, 31: 88–99. <https://doi.org/10.1557/jmr.2015.257>.
- [29] BABAK O, YULIA I, ROMAN K, LEMBIT K, GARCIA S E, DAYAN N, TORSTEN S, ANITA H, JENO G. Evolution of microstructure and hardness in aluminum processed by high pressure torsion extrusion [J]. *Materials Science and Engineering A*, 2019, 762: 1–10. <https://doi.org/10.1016/j.msea.2019.138074>.
- [30] VOJTICH D. Challenges for research and development of new aluminium alloys [J]. *Metalurgija*, 2010, 49: 181–185. <https://doi.org/10.1016/j.yimgme.2010.11.164>.
- [31] VIDYASAGAR C S, KARUNAKAR D B. Improvement of mechanical properties of 2024 AA by reinforcing yttrium and processing through spark plasma sintering [J]. *Arab J Sci Eng*, 2019, 44: 7859–7873. <https://doi.org/10.1007/s13369-019-03924-5>.
- [32] YAMAOGU R, OLEVSKY E A. Consolidation of Al-nano SiC composites by spark plasma sintering [J]. *Int J Mater Mech Manuf*, 2015, 4: 119–122. <https://doi.org/10.7763/ijmmm.2016.v4.237>.
- [33] DUTTA G, BOSE D. Effect of sintering temperature on density, porosity and hardness of a powder metallurgy component [J]. *Int J Emerg Technol Adv Eng*, 2012, 2: 121–123.
- [34] XU Z G, HODGSON M, CHANG K, CHEN G, YUAN X W, CAO P. Effect of sintering time on the densification, microstructure, weight loss and tensile properties of a powder metallurgical Fe–Mn–Si alloy [J]. *Metals (Basel)*, 2017, 7: 81. <https://doi.org/10.3390/met7030081>.
- [35] HE B B, HU B, YEN H W, CHENG G J, WANG Z K, LUO H W, HUANG M X. High dislocation density-induced large ductility in deformed and partitioned steels [J]. *Science*, 2017, 357: 1029–1032. <https://doi.org/10.1126/science.aan0177>.
- [36] VIDYASAGAR C S, KARUNAKAR D B. Effects of yttrium addition and aging on mechanical properties of AA2024 fabricated through multi-step stir casting [J]. *Trans Nonferrous Met Soc China*, 2020, 30: 288–302. [https://doi.org/10.1016/S1003-6326\(20\)65213-X](https://doi.org/10.1016/S1003-6326(20)65213-X).
- [37] NIU G, TANG Q, ZUROB H, WU H, XU L, GONG N. Strong and ductile steel via high dislocation density and heterogeneous nano/ultrafine grains [J]. *Materials Science and Engineering A*, 2019, 759: 1–10. <https://doi.org/10.1016/j.msea.2019.04.112>.
- [38] MUXIN Y, DINGSHUN Y, FUPING Y, PING J, EVAN M, XIAOLEI W. Dynamically reinforced heterogeneous grain structure prolongs ductility in a medium-entropy alloy with gigapascal yield strength [C]//*Proc Natl Acad Sci USA*, 2018, 115: 7224–7229. <https://doi.org/10.1073/pnas.1807817115>.

放电等离子烧结和冷轧 AA2024-Y 复合材料的力学性能和显微组织

CH. S. VIDYASAGAR¹, D. B. KARUNAKAR²

1. Metallurgical and Materials Engineering Department, Indian Institute of Technology, Roorkee-247667, India;

2. Mechanical and Industrial Engineering Department, Indian Institute of Technology, Roorkee-247667, India

摘要: 研究放电等离子烧结 AA2024-Y 复合材料低温轧制后的显微组织与力学性能的关系。添加钇有促进晶粒细化和析出的作用, 可以提高复合材料的力学性能; 但随着钇含量的增加, 力学性能有明显的先增加后减小的趋势。当钇含量为 0.3%(质量分数)时, 复合材料的力学性能最佳。为了进一步提高复合材料的抗拉强度, 在标准低温条件下对复合材料进行多道次低温轧制, 总压下量为 25%。对低温轧制后复合材料的力学性能及相应的显微组织进行研究。扫描电镜和透射电镜显微组织表明, 样品具有双尺寸晶粒, 即在实际晶粒内部形成纳米级的亚晶粒。低温轧制后, 由于晶粒尺寸的减小和位错密度的增加, 复合材料的拉伸性能明显提升; 添加 0.3%钇的复合材料具有最优的力学性能, 其硬度、屈服强度和极限抗拉强度分别为 HV 153、539 MPa 和 572MPa, 延展性适中。

关键词: 二次加工; 低温轧制; 纳米晶; 钇添加; 双尺寸晶粒; 放电等离子烧结

(Edited by Bing YANG)